RESEARCH ARTICLE • OPEN ACCESS

Hybrid ARIMA-Spatial Autocorrelation (Moran Index and LISA) for Covid-19 Vaccination in All Indonesian Provinces

Nur'ainul Miftahul Huda and Nurfitri Imro'ah

Volume 4, Issue 2, Pages 126–137, December 2023

Received 3 July 2023, Revised 5 October 2023, Accepted 21 December 2023, Published Online 31 December 2023

To Cite this Article : N. M. Huda and N. Imro'ah,"Hybrid ARIMA-Spatial Autocorrelation (Moran Index and LISA) for Covid-19 Vaccination in All Indonesian Provinces", *Jambura J. Biomath*, vol. 4, no. 2, pp. 126–137, 2023, *https://doi.org/10.37905/jjbm.v4i2.20915*

JOURNAL INFO • JAMBURA JOURNAL OF BIOMATHEMATICS

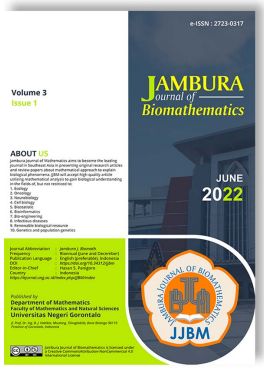

Homepage	:	http://ejurnal.ung.ac.id/index.php/JJBM/index
Journal Abbreviation	:	Jambura J. Biomath.
Frequency	:	Biannual (June and December)
Publication Language	:	English (preferable), Indonesia
DOI	:	https://doi.org/10.37905/jjbm
Online ISSN	:	2723-0317
Editor-in-Chief	:	Hasan S. Panigoro
Publisher	:	Department of Mathematics, Universitas Negeri Gorontalo
Country	:	Indonesia
OAI Address	:	http://ejurnal.ung.ac.id/index.php/jjbm/oai
Google Scholar ID	:	XzYgeKQAAAAJ
Email	:	editorial.jjbm@ung.ac.id

JAMBURA JOURNAL • FIND OUR OTHER JOURNALS

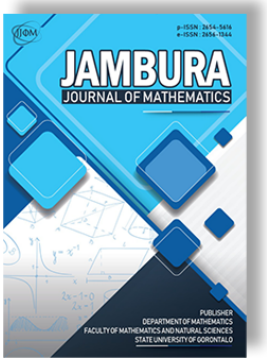

Jambura Journal of Mathematics

Jambura Journal of Mathematics Education

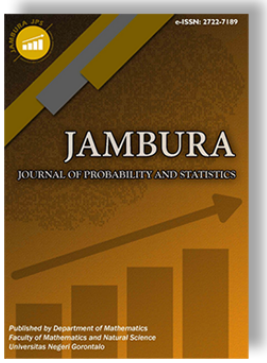

Jambura Journal of Probability and Statistics

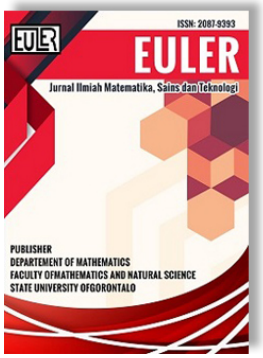

EULER : Jurnal Ilmiah Matematika, Sains, dan Teknologi

Jambura Journal of Biomathematics, Volume 4, Issue 2, Pages 126–137, December 2023 https://doi.org/10.37905/jjbm.v4i2.20915

Research Article

Check for updates

Hybrid ARIMA-Spatial Autocorrelation (Moran Index and LISA) for Covid-19 Vaccination in All Indonesian Provinces

Nur'ainul Miftahul Huda[1] **and Nurfitri Imro'ah**[2,*]

[1,2]*Mathematics Department, FMIPA, Universitas Tanjungpura, Pontianak 78124, Indonesia*

ARTICLE HISTORY
Received 3 July 2023
Revised 5 October 2023
Accepted 21 December 2023
Published 31 December 2023

KEYWORDS
forecasting
spatial autocorrelation
hybrid

ABSTRACT. *Numerous issues arise from stochastic processes with temporal and spatial index parameters. From 2020, Covid-19 has occurred worldwide. Combining time series with geographical analysis is crucial. ARIMA and spatial autocorrelation analysis using Moran's Index and LISA are prominent models for the two analyses. ARIMA predicts future values. The ARIMA model is applied to all recorded locations since it involves a stochastic process with a time and location parameter index. Then the prediction results at each location were examined using spatial autocorrelation, starting with the Moran index to see global relationships, then LISA (to look at the relationship between locations locally, to see which locations have a significant effect). The Queen Contiguity weight matrix calculates spatial autocorrelation (assuming that locations that are directly adjacent to each other have a spatial effect). Spatial autocorrelation will divide each place into four quadrants: High-High (HH), High-Low (HL), Low-High (LH), and Low-Low (LL). This approach was applied to 2021 Indonesian vaccination rates in all 34 provinces (354 days). Hence, the ARIMA model was applied to the 34 provinces, and each location received three forecasting. Moran's Index revealed spatial autocorrelation in the 354^{th} and 355^{th} time forecasts. LISA shows that Aceh (LL), West Sumatra (LH), South Sumatra (HH), Lampung (LH), and North Maluku (LL) influence other provinces (LH).*

1. Introduction

The approach of measuring spatial autocorrelation is an important one in quantitative analysis, particularly when viewed from a geographical prespective [1, 2]. This approach can serve as a foundation for spatial statistics when applied appropriately. The spatial technique is based on the first law of geography, which asserts that "everything is related to another, but things that are near are related more than those that are far" [3, 4]. These spatial qualities suggest that there is a dependence on space. When there is regular spatial variation in the values of a given variable, a phenomenon known as spatial autocorrelation is said to exist [5–7]. This variation can be broken down into two categories, which are known as positive and negative spatial autocorrelation, of between [8]. In the event that the autocorrelation is positive, the value variables at a certain location have a tendency to be comparable to the value variables in the surrounding area. If the values of numerous variables are found to be lower at a certain place, this denotes that the presence of spatial autocorrelation suggests that the value that is nearest to that position is also found to be lower [6, 9]. On the other hand, negative spatial autocorrelation is distinguished by the presence of distinct variance values at the site that is physically closest. For instance, when there is a negative spatial autocorrelation present, values with a low variation could be surrounded by values with a large variance at close places [10]. The term "positive spatial autocorrelation" refers to a pattern on a map in which geographic features that have the same value have a tendency to cluster on the map. On the other hand, the term "negative spatial autocorrelation" describes a pattern on a map in which geographic units that have similar values are distributed over the map [11]. Positive spatial autocorrelation happens when nearby environmental places have attribute values that are similar to one another [10, 12, 13].

The concept of spatial autocorrelation can be investigated from two different perspectives, namely, the local and the global [14]. Analysis of global autocorrelation entails looking at all of the different patterns on the maps [15]. The grouping or distribution of variations is typically what causes this global autocorrelation to give rise to problems in its use. On the other hand, local autocorrelation shifts focus to study more deeply global patterns to identify possible clusters, or that represent heterogeneity that deviates from global patterns [16]. This can be done by identifying probable clusters. The solution to many questions concerning the presence of spatial patterns can be found in global spatial autocorrelation [17]. Clustered as well as spread around the area. On the other hand, local provides solutions to location issues that have a considerable impact on the spatial patterns that exist (maps) [18]. Several approaches in spatial autocorrelation, including

1. The Gamma index of spatial autocorrelation, Moran's I, and Geary's C are examples of global spatial autocorrelation methods [19–21]
2. The Local Spatial Autocorrelation Index (LISA) and the Local Geary Index are both examples of local spatial autocorrela-

*Corresponding Author.

Email : *nurfitriimroah@math.untan.ac.id* (N. Imro'ah)
Homepage : http://ejurnal.ung.ac.id/index.php/JJBM/index / E-ISSN : 2723-0317

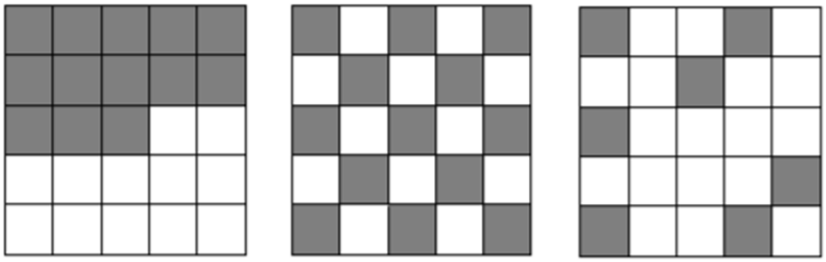

(a) positive (b) negative (c) zero

Figure 1. Illustration of autocorrelation

tion indicators [22, 23]

3. The variogram method for analyzing spatial connection from a geostatistical point of view, comprising the correlogram and semi-variogram [24–26]

In the field of geographic analysis, LISA was first presented by Luc Anselin as an extension of Moran's statistics [22], which had been conceived of and developed by Patrick Moran. When looking for statistically connected spatial autocorrelation on a global scale, Moran is a useful tool. whereas LISA is utilized to help in the formation of local spatial association patterns in mapped data and for the deconstruction of global autocorrelation measures, such as Moran statistics [27–29], Geary statistics [30], and Getis-Ord G statistics [31]. It is possible to think of LISA as a variation of the window-based Moran coefficient that was developed for pixels that are contained within a local region of an image [23]. A more succinct explanation would be to say that LISA is an advanced study that compares the qualities of one site with those of other nearby locations. In addition, LISA categorizes each place into one of four quadrants, labeled High-High (HH), High-Low (HL), Low-High (LH), and Low-Low (LL), respectively [32]. When applied to data on stationary time series, the Autoregressive Moving Average (ARIMA) models perform quite well. In time series analysis, it is common practice to make the assumption of stationarity. The ARIMA time series model's prediction performances are examined in this article using a spatial autocorrelation analysis. Future perception of the spatial relationship is its goal. The Box-Jenkins iterative process was used to create prediction results using the ARIMA time series model. In other words, based on the optimal ARIMA model at each location, this work presents a new method for identifying spatial autocorrelation. Several studies pertaining to the ARIMA model have advanced significantly [29, 33, 34]. The most recent research also incorporates spatial autocorrelation and GSTAR space-time analysis in Covid-19 instances [35].

Case studies of vaccine distribution in each province were employed in this study (in relative proportions to the population). Regarding vaccine distribution, vaccination-related issues in Indonesia are of the utmost importance. In each province, different data patterns can be identified. This is demonstrated by the uneven distribution of the vaccine throughout the population. Up to 50% of the recommended doses of the Covid-19 vaccination are distributed to each of the seven provinces on the islands of Java and Bali. Due to the comparatively high number of Covid-19 cases discovered in the islands of Java and Bali, the high distribution was caused. The remainder are dispersed throughout 27 more provinces that are not in Java or Bali. Another reason for the comparatively low vaccination rates in some areas is a lack of understanding of the value of vaccines. Vaccination and herd immunity are closely connected concepts. If more people were immune to the disease, it would be more harder for it to spread [36–39]. The percentage of the population that receives the vaccine will decide how much less frequently the disease occurs. A person's body will develop a specific immunity to diseases that can be prevented by vaccination after receiving a vaccination. The body will be better able to fight sickness as a result. These individuals' immune systems assault disease-causing germs or viruses when they attempt to infect them, preventing infection [40]. As a result, there will be a spatial effect that is proportional to the population immunised in a particular location on lowering Covid-19 instances in the closest location. This study aims to reveal which Indonesian provinces are noteworthy in terms of vaccine injections based on the results of ARIMA forecasting and to predict when vaccination will begin to have a spatial effect in each province. Also, this study uses the forecasting findings from ARIMA to examine the spatial connection of the specification level on a map for each province in Indonesia. The distribution of the assets will be displayed on the map.

2. Weight Matrix in Spatial

The correlation between variables and themselves that is based on space is known as spatial autocorrelation. Alternatively, spatial autocorrelation can be interpreted as a correspondence between the objects in the area. The values for spatial autocorrelation might vary anywhere from -1 to 1, inclusive. The neighboring places have values that are comparable to one another, which is typically indicative of positive spatial autocorrelation. On the other hand, sites that are near to one another have different values, which indicates that there is a negative spatial autocorrelation. In comparison, 0% spatial auto-correlation displays random location patterns. The examples of positive, negative, and zero auto-correlation are presented in Figures 1a to 1c [22].

In spatial data modeling, a key component is the spatial weighting matrix, which reflects the dependence in the data in a spatial context. The overarching structure of the spatial weight-

ing matrix, $\mathbf{W}_{n\times n}$, is [35]

$$\mathbf{W} = \begin{bmatrix} w_{11} & w_{12} & \dots & w_{1n} \\ w_{21} & w_{22} & \dots & w_{2n} \\ \vdots & \vdots & \ddots & \vdots \\ w_{n1} & w_{n2} & \dots & w_{nn} \end{bmatrix}$$

The elements of $\mathbf{W}$ are w_{ij}, where i and j is the row and column on the $\mathbf{W}$. All diagonal elements of w_{ij} are 0, whereas it is assumed that locations are not adjacent to the site itself. The w_{ij} comprises two values, particularly zero and one. One for the region that is adjacent, and zero for the areas that are not adjacent. The contiguity weight and the distance weight are the two primary categories of spatial weighting matrices. The link of the sides or vertices of one site to those of another site is what is meant by the term "contiguity weight." It is made up of a rook, a bishop, and a queen in close proximity to one another [22]. Figures 1a to 1c shows the illustration of contiguity weight. Based on those figures, let x_i be the i-th location for $i = 1, 2, \dots, 9$ and x_0 be the reference location. Using rock contiguity weight, the edges only $x_2; x_4; x_5; x_7$ are neighbors of x_0. While in bishop's contiguity weight, the corners only $x_1; x_3; x_6; x_8$ are neighbors of x_0. In contrast, the queen contiguity weight of the edges and corners x_0 has eight neighbors. In this study, the weight matrix used is the Queen Contiguity Matrix. Queen contiguity is the intersection of a site's sides and the corner point with another.

3. ARIMA - Spatial Autocorrelation (Moran Index and LISA)

A combination of time series modeling with spatial data modeling, the ARIMA Model - Spatial Autocorrelation is a powerful tool. The fundamental description of this modeling might be stated as [41]

1. The ARIMA model is applied to the modeling of time series data collected at each location. The model is applied so that prediction results can be obtained at each location. If there are four locations, then there will be four different ARIMA models (one model per location).
2. The results of the prediction for each place are then modeled spatially using the Moran Index and LISA so that the spatial correlation between locations and times may be examined. The Moran Index and the LISA are the two approaches that are used, and each of these methods is used to see global and local spatial correlations accordingly. Both of these methods are utilized.

The combination of these models enables the development of prediction results divided by time and location, as well as spatial correlation forecasts decomposed by time. Figure 2 provides further information regarding the modeling technique.

3.1. ARIMA

Let $\{\mathbf{Y}_t\} = [Y_{i,t}]$, for $i = 1, 2, \dots, N$ (locations) and $t = 1, 2, \dots, T$ (time), follows the ARIMA(p, d, q) model, then

$$\begin{aligned} \Phi_{i,p}(B)Y_{i,t} &= \Theta_{i,q}(B)e_{i,t}, \\ (1 - \phi_{i,1}B - \phi_{i,2}B^2 &= (1 - \theta_{i,1}B - \theta_{i,2}B^2 \\ -\dots - \phi_{i,p}B^p)Y_{i,t} &\quad -\dots - \theta_{i,q}B^q)e_{i,t}, \\ Y_{i,t} - \phi_{i,1}Y_{i,t-1} - \phi_{i,2}Y_{i,t-2} &= e_{i,t} - \theta_{i,1}e_{i,t-1} - \theta_{i,2}e_{i,t-2} \\ -\dots - \phi_{i,p}Y_{i,t-p} &\quad -\dots - \theta_{i,q}e_{t-q}, \end{aligned}$$

so that,

$$\begin{aligned} Y_{i,t} &= \phi_{i,1}Y_{i,t-1} + \phi_{i,2}Y_{i,t-2} + \dots + \phi_{i,p}Y_{i,t-p} + e_{i,t} \\ &\quad -\theta_1 e_{i,t-1} - \theta_2 e_{i,t-2} - \dots - \theta_q e_{t-q} \end{aligned} \tag{1}$$

where $\Phi_p = (1 - \phi_{i,1}B - \phi_{i,2}B^2 - \dots - \phi_{i,p}B^p)$, $\phi_{i,p}$ is autoregressive's parameter, $\Theta_{i,q}(B) = (1 - \theta_{i,1}B - \theta_{i,2}B^2 - \dots - \theta_{i,q}B^q)$, $\theta_{i,q}$ is moving average's parameter, B is backshift operator $(B^d Y_t = Y_{t-d})$, and $e_{i,t}$ is noise term for $i-th$ location and $t-th$ time.

In using the ARIMA model to analyze time series data using the Box-Jenkins method, it is assumed that the data must be stationary, i.e., have a constant mean and standard deviation. It is possible to conduct a test of stationarity using a variety of approaches, including a visual analysis based on plots, an autocorrelation function, or a unit root test, among others. Moreover, stationary data is modeled using the three-stage ARIMA Box-Jenkins, which includes [41]:

1. **Order Identification**, which involves deciding between the possible p, d, and q orders given the data. At this point, a number of possible orders are generated for use in subsequent parameter estimates and the decision of the most accurate model during the diagnostic test step. To identify the order, use Autocorrelation Function (ACF) and Partial ACF (PACF) plot from the data.

Table 1. Order Identification based on ACF and PACF

Model	ACF	PACF
AR(p)	tail off	cut off after lag p
MA(q)	cut off after lag q	tail off
ARMA(p, q)	tail off	tail off

2. The next step is called **parameter estimation**, and its purpose is to determine the values of the ARIMA model's parameters based on the orders that were found in the stage preceding it. Several ARIMA models were obtained at this point, which would subsequently undergo diagnostic testing.
3. **Diagnostic checking.** At this point, the model that will ultimately be chosen is determined. The assumption of **independence** between time lags (can be seen from ACF of residual) and **normality** (can be seen from normal q-q plot) needs to be satisfied by each and every residual value from the previous stages of the model. To put it another way, the model verifies that the **white noise assumption** is correct. The model that satisfies the white noise assumption as well as having the minimum Mean Square Error (MSE), Mean Absolute Percentage Error (MAPE), and Akaike Information Criterion (AIC) is the optimal model that can be utilized for prediction purposes.

3.2. Moran Index

The Moran's Index is a measurement of global spatial autocorrelation that is used to determine the existence or absence of a specific event. This is done by comparing the value of observations made at one location to those made at other sites that are close together at the same time [8]. Moran's Index examines the spatial autocorrelation, which reveals a relationship in which the significance of observations gathered at one site is contin-

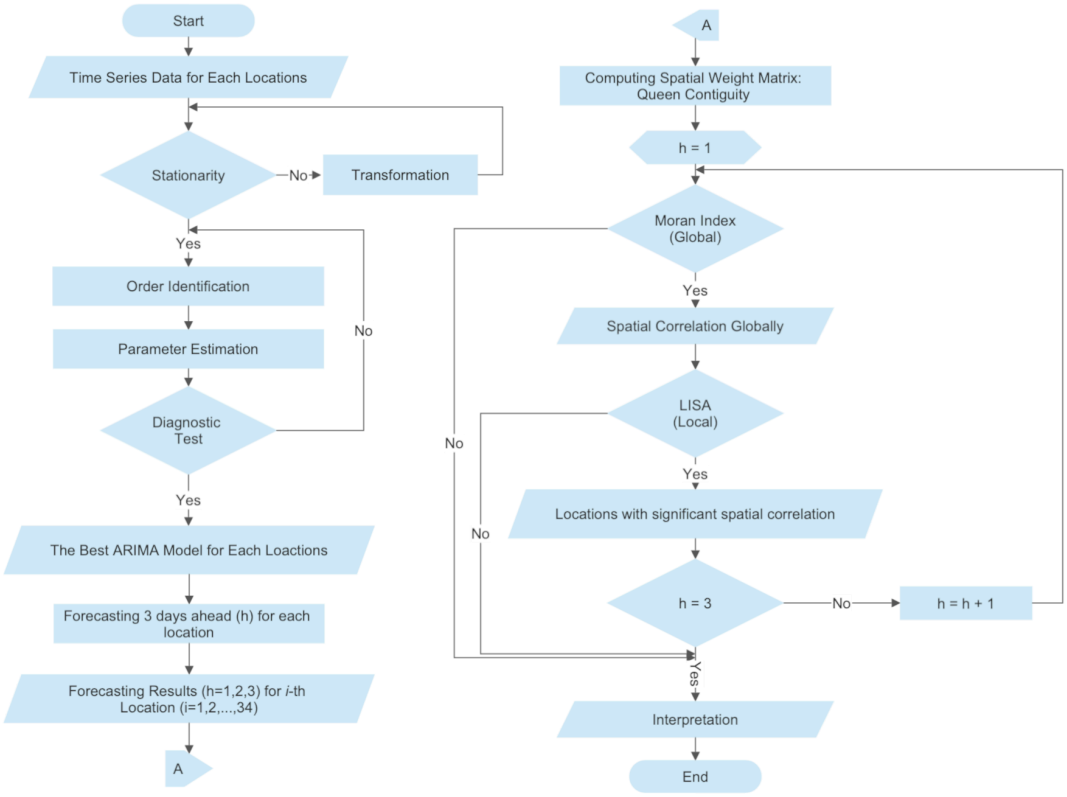

Figure 2. Flowchart of ARIMA-Spatial Autocorrelation

gent on the observations gathered at other sites located in close proximity to it. **The value of the Moran Index ranges between -1 and 1**. According to [22] Moran index can be measured using the equation [22]:

$$I = \frac{n\sum_{i=1}^{n}\sum_{j=1}^{n} w_{ij}(x_i - \bar{x})(x_j - \bar{x})}{\sum_{i=1}^{n}(x_i - \bar{x})^2},$$

where x_i is the value of observations in the $i-th$ region, $\bar{x}$ is the average number of events, w_{ij} is the element of the weighting matrix between area i and j.

The Moran's scatterplot (see Figure 3) is a tool that allows one to examine the link between standardized observation values and the standardized, average values of nearby areas. It is the first stage in getting across the statistics of the Moran's Index. The significance of the data is used to determine the position of the horizontal X-axis in Moran's scatterplot. The matching observation's weighted average or spatial lag on the horizontal X-axis serves as the basis for the calculation of the vertical Y-axis [8]. According to [22], the quadrants in the Moran's scatterplot are as follows:

(1) Quadrant I (High-High, HH) identifies areas with high surrounded by high observation values (yellow square in Figure 3)
(2) Quadrant 2 (Low-High, LH) identifies areas with low surrounded by high observation values (grey square in Figure 3)
(3) Quadrant III (Low-Low, LL) identifies areas with low surrounded by low observation values (blue square in Figure 3)
(4) Quadrant IV (High-Low, LL) identifies areas with high surrounded by low observation values (orange square in Figure 3)

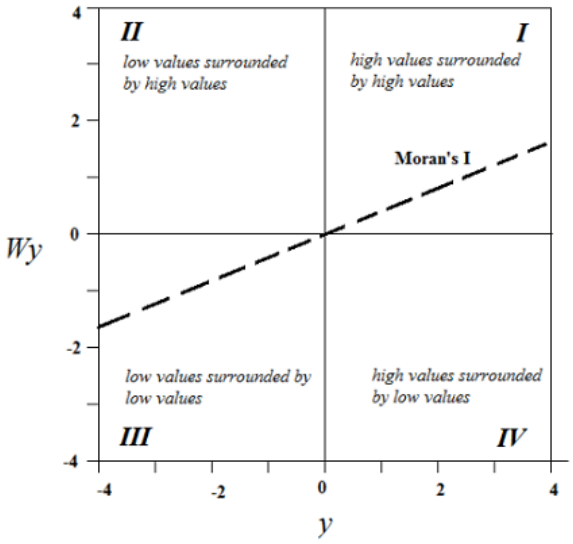

Figure 3. Moran's Scatterplot

The Moran Scatterplot, which places observations in quadrants I and III, demonstrates the presence of a positive spatial autocorrelation, which can be defined as the clustering of values that have the same high and low extremes. The Moran Scatterplot, on the other hand, arranges the observations in quadrants II and IV and reveals a negative spatial autocorrelation as well as distinct grouping values.

3.3. *Local Indicator of Spatial Autocorrelation (LISA)*

In this instance, the issue with global spatial autocorrelation is that Moran's Index does not provide any information on

Table 2. Notation for Each Location

No.	Variable	Province	No.	Variable	Province
1	$P_{1,t}^{(1)}$	Aceh	18	$P_{1,t}^{(3)}$	West Nusa Tenggara
2	$P_{2,t}^{(1)}$	West Sumatera	19	$P_{2,t}^{(3)}$	East Nusa Tenggara
3	$P_{3,t}^{(1)}$	South Sumatera	20	$P_{3,t}^{(3)}$	Papua
4	$P_{4,t}^{(1)}$	Riau Island	21	$P_{4,t}^{(3)}$	West Papua
5	$P_{5,t}^{(1)}$	North Sumatera	22	$P_{5,t}^{(3)}$	Maluku
6	$P_{6,t}^{(1)}$	Bengkulu	23	$P_{6,t}^{(3)}$	North Maluku
7	$P_{7,t}^{(1)}$	Jambi	24	$P_{1,t}^{(4)}$	South Sulawesi
8	$P_{8,t}^{(1)}$	Riau	25	$P_{2,t}^{(4)}$	Central Sulawesi
9	$P_{9,t}^{(1)}$	Bangka Island	26	$P_{3,t}^{(4)}$	Gorontalo
10	$P_{10,t}^{(1)}$	Lampung	27	$P_{4,t}^{(4)}$	West Sulawesi
11	$P_{1,t}^{(2)}$	Banten	28	$P_{5,t}^{(4)}$	South-East Sulawesi
12	$P_{2,t}^{(2)}$	Jakarta	29	$P_{6,t}^{(4)}$	North Sulawesi
13	$P_{3,t}^{(2)}$	West Java	30	$P_{1,t}^{(5)}$	East Kalimantan
14	$P_{4,t}^{(2)}$	Yogyakarta	31	$P_{2,t}^{(5)}$	West Kalimantan
15	$P_{5,t}^{(2)}$	Central Java	32	$P_{3,t}^{(5)}$	South Kalimantan
16	$P_{6,t}^{(2)}$	East Java	33	$P_{4,t}^{(5)}$	Central Kalimantan
17	$P_{7,t}^{(2)}$	Bali	34	$P_{5,t}^{(5)}$	North Kalimantan

the spatial patterns that are present in specific regions. As a result, employing the Local Indicator of Spatial Autocorrelation (LISA) to gather data on the pattern of spatial correlations in each site is necessary. According to [8], LISA identifies the relationship between one observation location and others. The LISA for each region i is written as follows [22]:

$$L_i = \frac{(x_i - \bar{x})}{\frac{1}{n}\sum_{i=1}^{n}(x_i - \bar{x})^2} \sum_{j=1}^{n} w_{ij}(x_j - \bar{x}),$$

where L_i is the LISA value in the $i-th$ region, n is the number of observations in the $i-th$ region, x_j is the value of observations in the $j-th$ region, $\bar{x}$ is the average number of events, w_{ij} is the element of the weighting matrix between area i and j.

4. Result and Discussion

4.1. Descriptive Statistics

The data used is the proportion of the population vaccinated with the first dose in all Indonesian provinces since January 13^{rd} - December 31^{st}, 2021 or 354 days (**time**)). There are 34 provinces used (**location**). Figure 4a shows the total population per province; the darker the color, the more densely populated the province is. In comparison, the proportion of vaccines is given in Figure 4b. The darker the color, the more the proportion of vaccines injected by the province. The mean and standard deviation of the data used is driven in Figure 4b.

The number of locations used are 34 locations. It means that there are 34 ARIMA model. To facilitate the presentation, the presentation of data is grouped by island. The notation of $P_{i,t}^{(k)}$ represents the variable at $i-$th location in $k-$th island at time t, for $k = 1, 2, \ldots, 5$, $i = 1, 2, \ldots, 10$, and $t = 1, 2, \ldots, 353$.

The existence of a strong correlation in time and space is one of the important premises upon which time series modeling and spatial modeling are constructed. Pearson's correlation is a useful tool for determining whether or not two locations are associated with one another before making any initial assumptions. More specifically, for time correlation, ARIMA time series modeling use a correlogram plot, and for spatial correlation, the Moran Index value. Figure 5 displays the findings of this study's application of Pearson's correlation analysis on Java (P2) data. The correlation coefficient between locations is demonstrated by the numbers that are given in Figure 5. For instance, in the first row of the third column, the number 0.84 is written. This indicates that the correlation between Banten and West Java areas in terms of the proportion of vaccines is 84%. In addition, the significance level is shown by the asterisk (*), which ranges from *** (99%), ** (95%), and * (90%). In addition to this, the scatter plot and the histogram of the data are presented in Figure 5.

4.2. ARIMA Model

The ARIMA time series modeling approach investigates historical data trends in its most fundamental form. As a result, a time series data plot is given for each site prior to engaging in ARIMA time series modeling. As can be seen in Table 1, the plots of the time series data for each site have been categorized according to the transmission of the islands. Hence, there are five different time series plots (see Figure 1). Interpretation. In the middle of the year, between June and July, there is an increase in the amount of data for each location. The same thing, a rise, took place toward the end of the year as it did before. This is inversely proportionate to the beginning of the year, when the percentage of people who have had their vaccinations is still relatively low. The month of March marked the beginning of the observed increases, particularly on the island of Java. When compared to Java Island, which has the highest level of vaccination awareness, the levels of vaccination awareness in Nusa Tenggara and Papua are very low. This is in contrast to Java Island, which has the highest level of vaccination awareness. The fact that Java Island serves as the administrative hub of the nation is one factor that may have an impact on this.

The assumption in ARIMA model is stationary. The stationarity test utilizing the Augmented Dickey Fuller (ADF) test on the

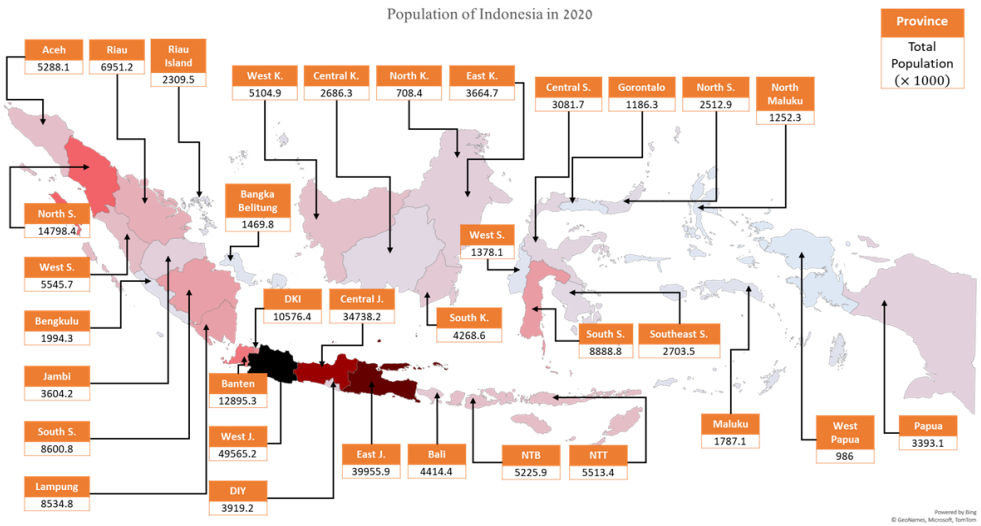

(a) The population of Indonesia (in 2020)

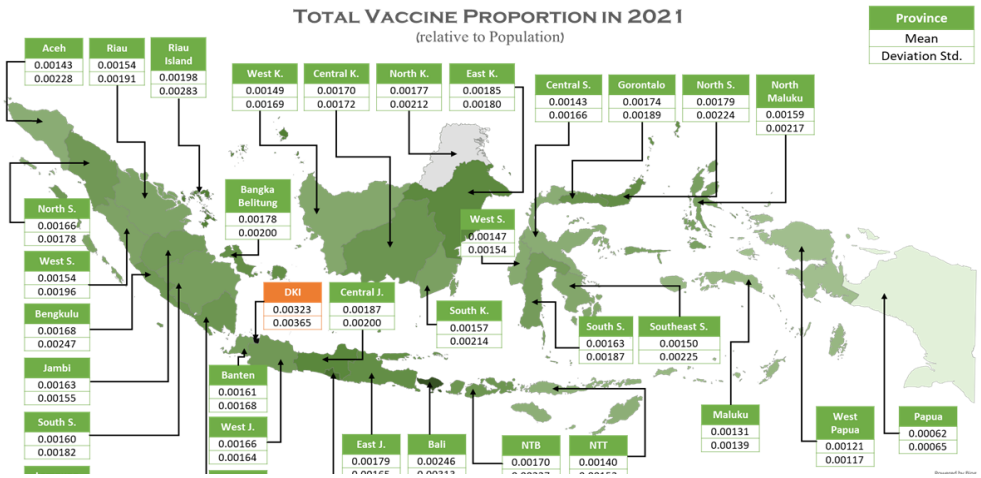

(b) Total vaccine proportion (in 2021)

Figure 4. Mapping of:

data for each site showed that the entire data are not stationary. This conclusion was reached after applying the test to each set of data. A differentiation process is applied to the data for each location just once as a consequence of this conclusion. In addition, the stationarity test was performed on differentiated data using the ADF test, and the conclusion reached was that the data for each site were stationary.

Based on the preceding stationarity process, the model created at each point might be ARIMA $(p, 1, q)$. At the stage of order identification, the ACF and PACF plots are analyzed in order to make a decision about the order in which p and q should be decided. The process of estimating parameters is not discussed in detail in this article, nor are any of the various different models that could be derived from each site. Following completion of all three Box-Jenkins phases for each location, the best model for each location is subsequently obtained (see Table 3).

Interpretation. According to Table 3, for the case of $k = 1$ (Sumatra Island) and $i = 1$ (Aceh), the best ARIMA model that can be produced is ARIMA(2,1,5), which means that

$$\begin{aligned} P_{1,t}^{(1)} \quad = \quad & -0.32P_{1,t-1}^{(1)} - 0.75P_{1,t-2}^{(1)} + 0.02e_{1,t-1}^{(1)} - 0.77e_{1,t-2}^{(1)} \\ & +0.29e_{1,t-3}^{(1)} - 0.03e_{1,t-4}^{(1)} + 0.28e_{1,t-5}^{(1)}. \end{aligned}$$

This indicates that the proportion of people who have received vaccines in Aceh one and two days ago (at times $t-1$ and $t-2$) has an effect on the proportion of people who have received vaccinations today (at time t). In addition to that, it is also impacted by errors that occurred between 1 and 5 days ago (at times $t-1, t-2, \ldots, t-5$). For the remaining locations, the ARIMA model conforms to the ARIMA order and is described based on eq. (1).

Prediction is the last stage of the ARIMA modeling approach for time series. Afterwards, the results of this prediction will be utilized to examine the spatial autocorrelation that exists between diverse locations $(\hat{P}_{i,354+h}^{(k)})$. On the basis of each ARIMA model at each location, forecasts are generated for three different times $(h = 1, 2, 3)$ in the future. Table 4 offers a comprehensive presentation of the results of the predicted for each location.

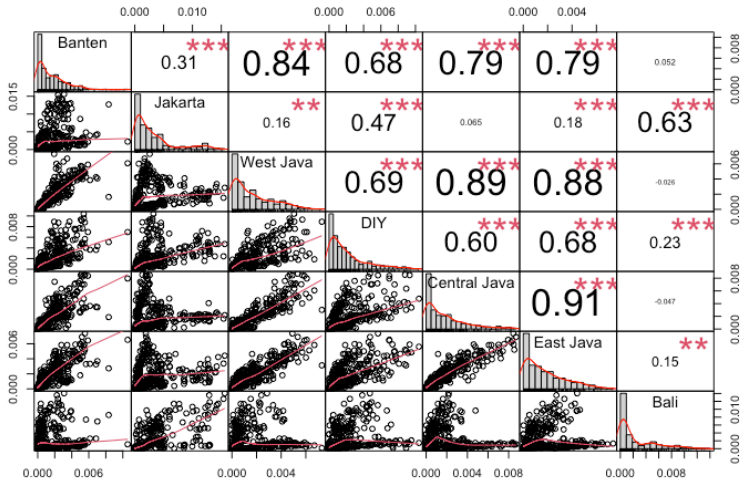

Figure 5. Correlation among Locations in Java Island

Table 3. Parameter Estimation of ARIMA(p,1,q) Model for 34 Locations

Loc.	Ordo	Autoregressive (AR)					Moving Average (MA)				
		ϕ_1	ϕ_2	ϕ_3	ϕ_4	ϕ_5	θ_1	θ_2	θ_3	θ_4	θ_5
$P_{1,t}^{(1)}$	$(2,1,5)$	-0.32	-0.75				-0.02	0.77	-0.29	0.03	-0.28
$P_{2,t}^{(1)}$	$(1,1,1)$	-0.26					-0.73				
$P_{3,t}^{(1)}$	$(4,1,2)$	-0.71	0.04	-0.12	-0.23		0.19	-0.54			
$P_{4,t}^{(1)}$	$(0,1,2)$						-0.81	0.13			
$P_{5,t}^{(1)}$	$(1,1,1)$	0.35					-0.83				
$P_{6,t}^{(1)}$	$(4,1,5)$	-0.54	0.24	-0.53	-0.94		-0.11	-0.51	0.50	0.46	-0.43
$P_{7,t}^{(1)}$	$(4,1,3)$	-0.36	0.23	-0.54	-0.68	-0.31	-0.37	0.57			
$P_{8,t}^{(1)}$	$(0,1,3)$						-0.45	0.13	-0.16		
$P_{9,t}^{(1)}$	$(4,1,3)$	-0.10	0.19	-0.60	-0.51		-0.48	-0.30	0.79		
$P_{10,t}^{(1)}$	$(4,1,3)$	-0.17	-0.39	0.47	0.38		-0.32	0.32	-0.83		
$P_{1,t}^{(2)}$	$(1,1,1)$	0.44					-0.87				
$P_{2,t}^{(2)}$	$(2,1,2)$	1.11	-0.66				-1.57	0.80			
$P_{3,t}^{(2)}$	$(2,1,3)$	-1.18	-0.61				0.47	-0.18	-0.74		
$P_{4,t}^{(2)}$	$(4,1,3)$	-0.34	0.21	-0.59	-0.72		-0.30	-0.21	0.64		
$P_{5,t}^{(2)}$	$(2,1,3)$	-1.42	-0.72				0.63	-0.26	-0.74		
$P_{6,t}^{(2)}$	$(4,1,3)$	-0.33	0.23	-0.56	-0.73		-0.43	-0.29	0.66		
$P_{7,t}^{(2)}$	$(2,1,4)$	-0.95	-0.63				0.45	-0.01	-0.62	0.01	
$P_{1,t}^{(3)}$	$(0,1,1)$						-0.69				
$P_{2,t}^{(3)}$	$(0,1,2)$						-0.60	-0.16			
$P_{3,t}^{(3)}$	$(0,1,1)$						-0.61				
$P_{4,t}^{(3)}$	$(0,1,1)$						-0.77				
$P_{5,t}^{(3)}$	$(2,1,5)$	-0.39	-0.75				-0.20	0.65	-0.65	0.00	-0.50
$P_{6,t}^{(3)}$	$(0,1,1)$						-0.29				
$P_{1,t}^{(4)}$	$(1,1,5)$	0.44					-1.05	0.38	0.07	-0.56	0.48
$P_{2,t}^{(4)}$	$(0,1,1)$						-0.60				
$P_{3,t}^{(4)}$	$(2,1,5)$	-0.20	0.46				-0.39	-0.72	0.08	0.02	0.28
$P_{4,t}^{(4)}$	$(2,1,1)$	0.19	0.23				-0.86				
$P_{5,t}^{(4)}$	$(0,1,1)$						-0.53				
$P_{6,t}^{(4)}$	$(5,1,2)$	0.09	-0.69	-0.35	-0.33	-0.50	-0.63	0.60			
$P_{1,t}^{(5)}$	$(4,1,3)$	-0.25	0.22	-0.57	-0.57		-0.46	-0.25	0.66		
$P_{2,t}^{(5)}$	$(5,1,2)$	0.34	-0.58	-0.31	-0.27	-0.29	-0.83	0.69			
$P_{3,t}^{(5)}$	$(2,1,3)$	0.91	-0.64				-1.37	1.27	-0.60		
$P_{4,t}^{(5)}$	$(5,1,2)$	-0.55	0.30	-0.05	-0.28	0.20	-0.11	-0.61			
$P_{5,t}^{(5)}$	$(3,1,3)$	-1.34	-0.20	0.42			0.80	-0.66	-0.76		

Table 4. Forecasting Results for 3 Steps Ahead based on ARIMA(p,d,q) Model for 34 Locations

Location	Forecasting ($\hat{P}^{(k)}_{i,354+h}$)			Location	Forecasting ($\hat{P}^{(k)}_{i,354+h}$)		
	$h=1$	$h=2$	$h=3$		$h=1$	$h=2$	$h=3$
$\hat{P}^{(1)}_{1,354+h}$	0.0014	0.0020	0.0017	$\hat{P}^{(3)}_{1,354+h}$	0.0019	0.0019	0.0019
$\hat{P}^{(1)}_{2,354+h}$	0.0012	0.0014	0.0013	$\hat{P}^{(3)}_{2,354+h}$	0.0013	0.0013	0.0013
$\hat{P}^{(1)}_{3,354+h}$	0.0037	0.0028	0.0031	$\hat{P}^{(3)}_{3,354+h}$	0.0003	0.0003	0.0003
$\hat{P}^{(1)}_{4,354+h}$	0.0021	0.0020	0.0020	$\hat{P}^{(3)}_{4,354+h}$	0.0011	0.0011	0.0011
$\hat{P}^{(1)}_{5,354+h}$	0.0051	0.0048	0.0047	$\hat{P}^{(3)}_{5,354+h}$	0.0051	0.0046	0.0042
$\hat{P}^{(1)}_{6,354+h}$	0.0039	0.0018	0.0025	$\hat{P}^{(3)}_{6,354+h}$	0.0006	0.0007	0.0006
$\hat{P}^{(1)}_{7,354+h}$	0.0025	0.0015	0.0017	$\hat{P}^{(4)}_{1,354+h}$	0.0024	0.0022	0.0018
$\hat{P}^{(1)}_{8,354+h}$	0.0019	0.0020	0.0018	$\hat{P}^{(4)}_{2,354+h}$	0.0012	0.0012	0.0012
$\hat{P}^{(1)}_{9,354+h}$	0.0047	0.0029	0.0026	$\hat{P}^{(4)}_{3,354+h}$	0.0011	0.0008	0.0010
$\hat{P}^{(1)}_{10,354+h}$	0.0040	0.0045	0.0038	$\hat{P}^{(4)}_{4,354+h}$	0.0027	0.0027	0.0026
$\hat{P}^{(2)}_{1,354+h}$	0.0014	0.0016	0.0017	$\hat{P}^{(4)}_{5,354+h}$	0.0017	0.0017	0.0017
$\hat{P}^{(2)}_{2,354+h}$	0.0013	0.0014	0.0014	$\hat{P}^{(4)}_{6,354+h}$	0.0037	0.0031	0.0013
$\hat{P}^{(2)}_{3,354+h}$	0.0017	0.0021	0.0027	$\hat{P}^{(5)}_{1,354+h}$	0.0027	0.0013	0.0014
$\hat{P}^{(2)}_{4,354+h}$	0.0021	0.0003	0.0008	$\hat{P}^{(5)}_{2,354+h}$	0.0020	0.0012	0.0005
$\hat{P}^{(2)}_{5,354+h}$	0.0015	0.0022	0.0030	$\hat{P}^{(5)}_{3,354+h}$	0.0018	0.0016	0.0016
$\hat{P}^{(2)}_{6,354+h}$	0.0039	0.0014	0.0020	$\hat{P}^{(5)}_{4,354+h}$	0.0028	0.0018	0.0027
$\hat{P}^{(2)}_{7,354+h}$	0.0006	0.0007	0.0007	$\hat{P}^{(5)}_{5,354+h}$	0.0035	0.0021	0.0035

4.3. Spatial Autocorrelation - Moran Index and LISA

In the process of measuring spatial autocorrelation, one of the most significant procedures is the calculation of the weight matrix, which is also sometimes referred to as the queen contiguity matrix. The number one is assigned to the provinces that are immediately adjacent to one another, whereas the number zero is assigned to the remaining provinces. For instance, the province of Central Kalimantan (x_0) is given a value of 1 in relation to the provinces of West Kalimantan (x_1), East Kalimantan (x_2), and South Kalimantan (x_3). Since these provinces are directly adjacent to Central Kalimantan, they are each given a value of 1 in relation to Central Kalimantan. In the event that a province is not immediately next to another province, the number of transportation routes that may be rerouted to reach that province is one of the criteria that is used to decide whether or not that province can be released. For instance, the province of Maluku (y_0) is made up of a number of smaller islands, and there are no provinces that lie immediately to their immediate north or south. Maluku province, on the other hand, is accessible by road, air, and sea and may be reached via South Sulawesi (y_1) and North Maluku (y_2, respectively). Because of this, the rank of number 1 has been given to both of the provinces in this scenario. Figure 7 offers a graphical representation of the two scenarios that were mentioned earlier.

Based on the weight matrix calculation grid using queen contiguity, the following queen contiguity matrix is obtained

$$\mathbf{Q} = \begin{bmatrix} \mathbf{P}^{(1)} & \mathbf{O} & \mathbf{O} & \mathbf{O} & \mathbf{O} \\ \mathbf{O} & \mathbf{P}^{(2)} & \mathbf{O} & \mathbf{O} & \mathbf{O} \\ \mathbf{O} & \mathbf{O} & \mathbf{P}^{(3)} & \mathbf{O} & \mathbf{O} \\ \mathbf{O} & \mathbf{O} & \mathbf{O} & \mathbf{P}^{(4)} & \mathbf{O} \\ \mathbf{O} & \mathbf{O} & \mathbf{O} & \mathbf{O} & \mathbf{P}^{(5)} \end{bmatrix}$$

where $\mathbf{O}$ is a zero matrix, and

$$\mathbf{P}^{(1)} = \begin{bmatrix} 0&1&0&0&0&0&0&0&0&0 \\ 1&0&1&1&0&0&0&0&0&0 \\ 0&1&0&1&0&0&1&1&0&0 \\ 0&1&1&0&1&0&1&0&0&0 \\ 0&0&0&1&0&0&0&0&0&0 \\ 0&0&0&0&0&0&1&1&1&1 \\ 0&0&1&1&0&1&0&1&0&0 \\ 0&0&1&0&0&1&1&0&0&1 \\ 0&0&0&0&0&1&0&0&0&0 \\ 0&0&0&0&0&1&0&1&0&0 \end{bmatrix};$$

$$\mathbf{P}^{(2)} = \begin{bmatrix} 0&1&1&0&0&0&0 \\ 1&0&1&0&0&0&0 \\ 1&1&0&1&0&0&0 \\ 0&0&1&0&1&1&0 \\ 0&0&0&1&0&0&0 \\ 0&0&0&1&0&0&1 \\ 0&0&0&0&0&1&0 \end{bmatrix};$$

$$\mathbf{P}^{(3)} = \begin{bmatrix} 0&1&0&0&0&0 \\ 1&0&0&0&0&0 \\ 0&0&0&1&0&0 \\ 0&0&1&0&0&0 \\ 0&0&0&0&0&1 \\ 0&0&0&0&1&0 \end{bmatrix};$$

$$\mathbf{P}^{(4)} = \begin{bmatrix} 0&1&0&1&1&0 \\ 1&0&1&1&1&0 \\ 0&1&0&0&0&1 \\ 1&1&0&0&0&0 \\ 1&1&0&0&0&0 \\ 0&0&1&0&0&0 \end{bmatrix};$$

$$\mathbf{P}^{(5)} = \begin{bmatrix} 0&1&1&1&1 \\ 1&0&0&1&1 \\ 1&0&0&1&0 \\ 1&1&1&0&0 \\ 1&1&0&0&0 \end{bmatrix}.$$

$\mathbf{P}_1$ represents weigth block matrix for Sumatera's Island (Blue in Figure 7), $\mathbf{P}_2$, $\mathbf{P}_3$ consecutively represent Java (Red in Figure 7)and Kalimantan's Island (Yellow in Figure 7). The black in Figure 7 represent Sulawesi's Island, Maluku and North Maluku for $\mathbf{P}_4$. Then, $\mathbf{P}_5$ represents West Nusa Tenggara, East Nusa Tenggara, Papua, and West Papua. The following step is to standardize the $\mathbf{Q}$ matrix by making the number of each row 1, $\mathbf{Q}^*$. The standardized matrix is used as a weight matrix in calculating the Moran and local Moran index (LISA) values.

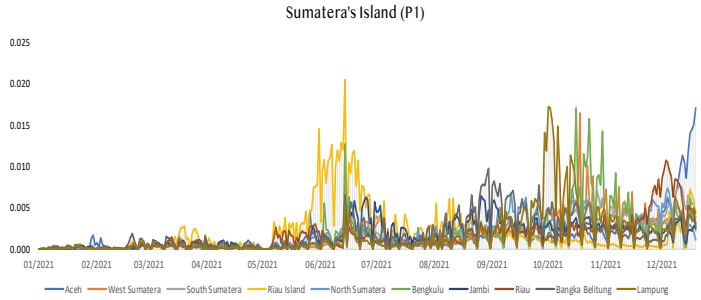

(a) Sumatera

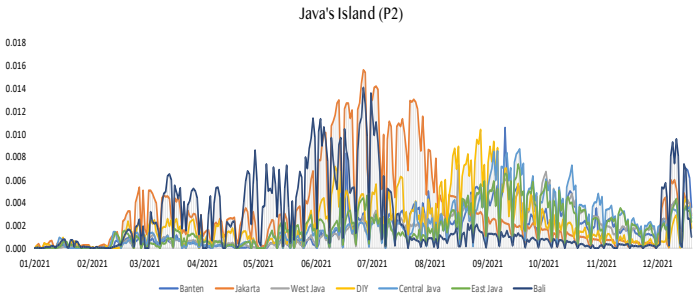

(b) Java

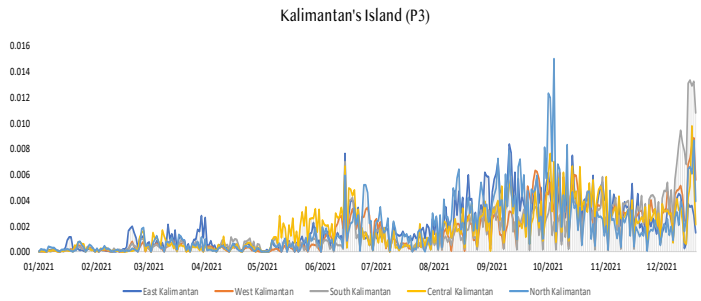

(c) Kalimantan

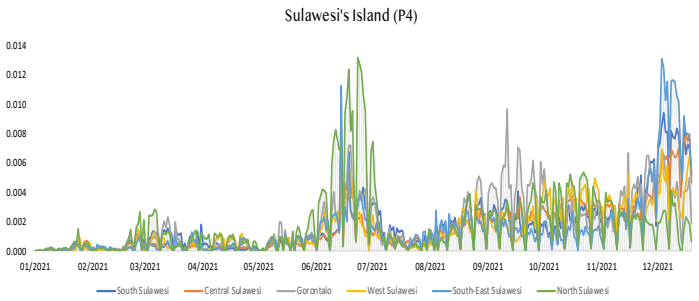

(d) Sulawesi

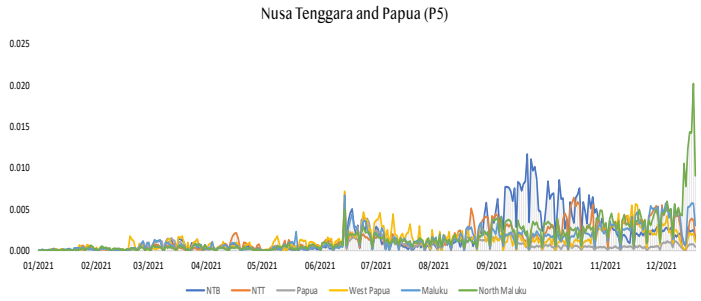

(e) Nusa Tenggara and Papua

Figure 6. Time Series Plot for Each Island

4.4. Moran's Index

The next step is to calculate the global spatial auto-correlation using the Moran's Index method for all t. The following is the calculation of the spatial auto-correlation using the Moran's Index for all t:

$$I_{354+h} = \frac{34\sum_{i=1}^{34}\sum_{j=1}^{34} q_{ij}^{*}(\hat{P}_{i,354+h} - \bar{P})(\hat{P}_{j,354+h} - \bar{P})}{S_0 \sum_{i=1}^{34}(\hat{P}_{i,t+h} - \bar{P})^2} \tag{2}$$

where q_{ij}^{*} is the weight for i-th to j-th location, $\bar{P}$ is the average proportion of vaccines across 34 provinces, $\hat{P}_{i,354+h}$ is the proportion of vaccines at i-th location, and $h = 1, 2, 3$.

It is crucial to make sure that the Moran Index performs a calculation of the global spatial autocorrelation. The ARIMA model will be utilised to make a prediction regarding the percentage of vaccines that will be given out, and the spatial auto-correlation will then be established on the basis of the results of the prediction. After that, the Moran Index can be calculated for each individual forecast outcome during the course of the following three days by making use of the eq. (2). The results of computing the Moran Index for each of the prediction times are listed in the table that can be found in Table 5. The global geographic correlation on the first day of predictions is 0.472, as shown in the Moran Index column, which depicts global geographical correlation. This can be seen by looking at the global spatial correlation. This suggests that the aggregate percentage of individuals who have received vaccinations across all of Indonesia's provinces is 47.2%. Because the p-value for the Moran Index on that day was 4.8 %, which is less than 5%, it is feasible to reach the conclusion that there is a substantial link between the percentage of people who have been vaccinated and the geographical location. On the other hand, the spatial correlation based on the Moran Index was -0.038 on the third day $(354 + 3)$, with a p-value (3.7%) that was greater than 5 %. This was shown to be the case on the third day $(354 + 3)$. In other words, the geographical correlation on the third day of prediction does not have a substantial influence on the outcome of the forecast. In light of this, the projection of the

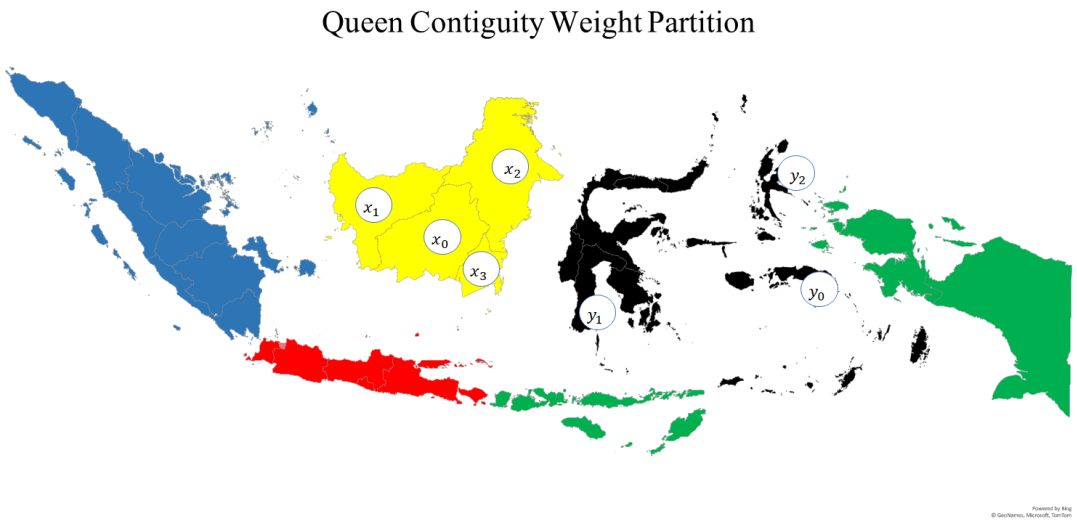

Figure 7. Illustration of Computing the Queen Contiguity

proportion of vaccines that were given out on the third day will not be affected by the computation of the spatial correlation that will be performed using LISA.

Table 5. Moran Index for each Forecasting Result based on ARIMA Model

Time $(354+h)$	Moran Index	p-value
I_{354+1}	0.472	0.048
I_{354+2}	0.374	0.029
I_{354+3}	-0.038	0.366

4.5. LISA

The only thing that can be determined from the outcomes of Moran's computation is whether or not there is a strong spatial auto-correlation. On the other hand, information that would have shown which places were responsible for the large spatial auto-correlation was left out. Despite this, additional research employing LISA was carried out in order to resolve this issue. The spatial auto-correlation value was computed in LISA for each province for each day that was significant (Moran's finding, see Table 5). The LISA for each day in the $i-th$ province can be calculated as follows:

$$L_{i,354+h} = \frac{(\hat{P}_{i,354+h} - \bar{P})}{\frac{1}{34}\sum_{i=1}^{34}(\hat{P}_{i,354+h} - \bar{P})^2} \sum_{j=1}^{34} w_{ij}(\hat{P}_{j,354+h} - \bar{P})$$

Based on the LISA calculations, the significant provinces in each significant's date are shown in Figure 8. The offered colors each represent a different class for the four quadrants. The Low-Low (LL), High-High (HH), High-Low (HL), and Low-High (LH) grades are denoted by the colors green, red, yellow, and orange, respectively. According to one possible interpretation of the significant LISA value, the province exerts a significant level of influence over the other provinces that are located in close proximity to it. For instance, on day 355, five different provinces, Aceh (LL), West Sumatera (LH), South Sumatera (HH), Lampung (LH) and North Maluku (LH), had significant LISA score (p-value less than 5%).

5. Conclusion

The findings of the ARIMA modelling performed in each location indicate that the mean does not exhibit stationary behaviour. Evenness is a characteristic of stationarity. This indicates that when the data is not stationary, it is possible to draw the conclusion that there are oscillations in the distribution of the vaccine. This can be brought about by a variety of factors, such as the progressive delivery of the vaccine, followed by the implementation of regulations that mandate vaccinations, and finally the requirement for the vaccine itself. ARIMA modelling carried out at each location reveals, among other things, the features of each location, which are almost always distinct from one another. This is demonstrated by the fact that the ARIMA models come in a variety of orders; some contain simply the MA or AR models, while others contain a combination of the two, denoted by the acronym ARMA. The ARIMA models are used to make predictions that are carried out three times further into the future at each location. After that, these findings are utilised in the subsequent geographical analysis, specifically the Moran Index and the LISA.

Moran's index has the capability of determining whether or not vaccination injections have a geographical influence on the relationships that exist between provinces. For each location, the projected results are used in the calculation of Moran's index, which is performed three times in advance. It was discovered that the results gathered on days 365 and 366 contained a significant Moran's index. Following the completion of general detection for all of the cases in which significance was discovered, targeted detection was carried out in order to establish which provinces had a major influence on increasing the quantity of vaccines provided each day. As many as five provinces, namely Aceh (LL), West Sumatra (LH), South Sumatra (HH), Lampung (LH), and North Maluku (LH), have been able to contribute to a reduction in the number of cases of the Covid-19 virus as a result of their participation in the Covid-19 killing programme. Four of the five provinces are located on the island of Sumatra. The other provinces are located on the other two islands. This suggests that the island of Sumatra has made a significant contribution to the suppression of the Covid-19 case through the implementation of immunisation programmes. Specifically in the province of South

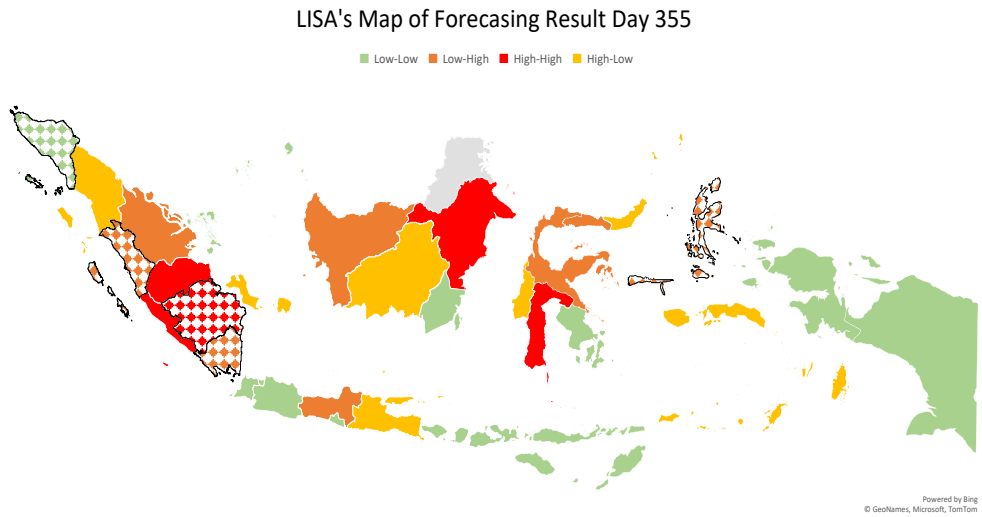

(a) Day 355

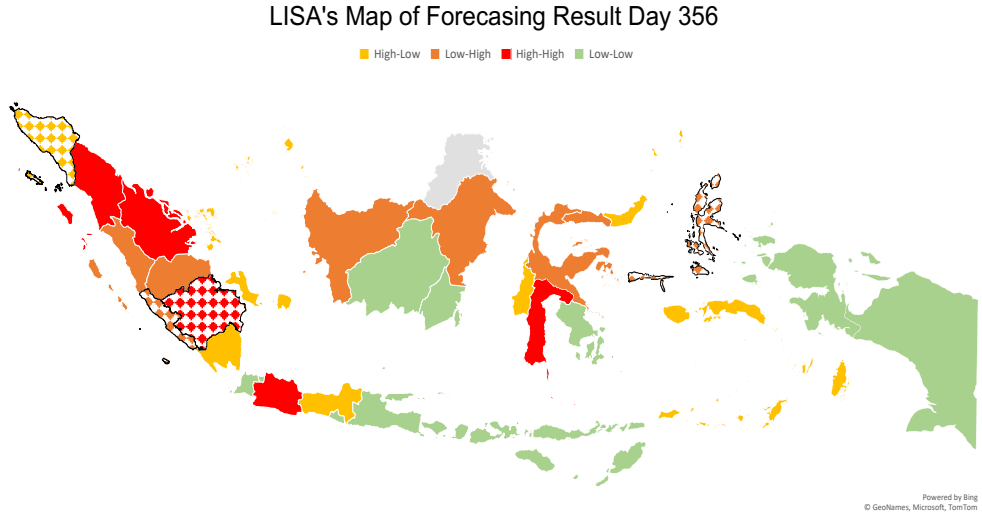

(b) Day 356

Figure 8. LISA's Map of Forecasting Result based on ARIMA and Moran Index

Sumatra, which can be found in the High-High quadrant. This implies that it is placed in an area that has a high proportion of vaccines and is located in closeness to other regions that also have a high proportion of vaccinations. Calculations of spatial autocorrelation that are based on these prediction results can be used as a reference in the distribution of vaccines, particularly for the purpose of determining which locations are appropriate to focus on in suppressing Covid-19 cases, specifically locations that are in the Low-Low quadrant of the map.

Author Contributions. **Huda, N. M.**: Conceived and designed the experiments; Analyzed and interpreted the data; Contributed reagents, materials, analysis tools or data; Wrote the paper. **Imro'ah, N.**: Conceived and designed the experiments; Performed the experiments; Analyzed and interpreted the data; Contributed reagents, materials, analysis tools or data; Wrote the paper.

Acknowledgement. The authors are thankful the editors and reviewers who have supported us in improving this manuscript and also to Kementerian Kesehatan Indonesia for the data.

Funding. This research received no external funding

Conflict of interest. The authors declare no conflict of interest

Data availability. The data was available online daily at https://vaksin.kemkes.go.id/#/vaccines

References

[1] Y. Chen, "An analytical process of spatial autocorrelation functions based on moran's index," *PLOS ONE*, vol. 16, no. 4, p. e0249589, 2021. DOI:10.1371/journal.pone.0249589

[2] Y. Chen, "Fractal analytical approach of urban form based on spatial correlation function," *Chaos, Solitons & Fractals*, vol. 49, pp. 47–60, 2013. DOI:10.1016/j.chaos.2013.02.006

[3] D. Z. Sui, "Tobler's first law of geography: A big idea for a small world?" *Annals of the Association of American Geographers*, vol. 94, no. 2, pp. 269–277, 2004. DOI:10.1111/j.1467-8306.2004.09402003.x

[4] B. Zheng, X. Lin, D. Yin, and X. Qi, "Does tobler's first law of geography apply to internet attention? a case study of the asian elephant

northern migration event," *PLOS ONE*, vol. 18, no. 3, p. e0282474, 2023. DOI:10.1371/journal.pone.0282474

[5] D. A. Griffith, "Spatial autocorrelation," *Encyclopedia of Social Measurement*, pp. 581–590, 2005. DOI:10.1016/B0-12-369398-5/00334-0

[6] A. Getis, "Spatial pattern analysis,"*Encyclopedia of Social Measurement*, pp. 627–632, 2005. DOI:10.1016/B0-12-369398-5/00336-4

[7] R. Haining, "Spatial autocorrelation,"*International Encyclopedia of the Social & Behavioral Sciences*, pp. 14763–14768, 2001. DOI:10.1016/B0-08-043076-7/02511-0

[8] S.-I. Lee, "Correlation and spatial autocorrelation,"Springer, 2017, pp. 360–368. ISBN 978-3-319-17884-4. DOI:10.1007/978-3-319-17885-1_1524

[9] R. Westerholt, "Exploratory statistical analysis of spatial structures in urban datasets," *Metropolitan Research: Methods and Approaches*, pp. 37–62, 2022. DOI:10.14361/9783839463109-003

[10] D. A. Griffith and G. Arbia, "Detecting negative spatial autocorrelation in georeferenced random variables," *International Journal of Geographical Information Science*, vol. 24, no. 3 pp. 417–437, 2010. DOI:10.1080/13658810902832591

[11] Y. H. Chou, "Map resolution and spatial autocorrelation," *Geographical Analysis*, vol. 23, no. 3, pp. 228–246, 1991. DOI:10.1111/j.1538-4632.1991.tb00236.x

[12] M. Almeida-Neto and T. M. Lewinsohn, "Small-scale spatial autocorrelation and the interpretation of relationships between phenological parameters," *Journal of Vegetation Science*, vol. 15, no. 4, pp. 561–568, 2004. DOI:10.1111/j.1654-1103.2004.tb02295.x

[13] G. W. Mueller-Warrant, G. W. Whittaker, and W. C. Young, "Gis analysis of spatial clustering and temporal change in weeds of grass seed crops," *Weed Science*, vol. 56, no. 5, pp. 647–669, 2008. DOI:10.1614/WS-07-032.1

[14] A. Getis, "A history of the concept of spatial autocorrelation: A geographer's perspective," *Geographical Analysis*, vol. 40, no. 3, pp. 297–309, 2008. DOI:10.1111/j.1538-4632.2008.00727.x

[15] L. M. Scott, "Spatial pattern, analysis of," *International Encyclopedia of the Social & Behavioral Sciences (Second Edition)*, pp. 178–184, 2015. DOI:10.1016/B978-0-08-097086-8.72064-2

[16] J. K. Ord and A. Getis, "Testing for local spatial autocorrelation in the presence of global autocorrelation," *Journal of Regional Science*, vol. 41, no. 3, pp. 411–432, 2002. DOI:10.1111/0022-4146.00224

[17] A. Fotheringham and P. Rogerson, *The SAGE Handbook of Spatial Analysis*. SAGE Publications, Ltd, 2009. ISBN 9781412910828

[18] A. R. Holt, M. Mears, L. Maltby, and P. Warren, "Understanding spatial patterns in the production of multiple urban ecosystem services," *Ecosystem Services*, vol. 16, pp. 33–46, 2015. DOI:10.1016/j.ecoser.2015.08.007

[19] J. Dubé and D. Legros, "Spatial autocorrelation," John Wiley & Sons, Ltd., *Spatial Econometrics Using Microdata*, 2014, pp. 59–91. ISBN 9781119008651. DOI:10.1002/9781119008651.ch3

[20] A. Abdulhafedh, "A novel hybrid method for measuring the spatial autocorrelation of vehicular crashes: Combining moran's index and getis-ord statistic," *Open Journal of Civil Engineering*, vol. 07, no. 2, pp. 208–221, 2017. DOI:10.4236/ojce.2017.72013

[21] A. Getis, "Reflections on spatial autocorrelation," *Regional Science and Urban Economics*, vol. 37, no. 4, pp. 491–496, 2007. DOI:10.1016/j.regsciurbeco.2007.04.005

[22] L. Anselin, "Local indicators of spatial association-lisa," *Geographical Analysis*, vol. 27, no. 2, pp. 93–115, 1995. DOI:10.1111/j.1538-4632.1995.tb00338.x

[23] M. Osadebey, M. Pedersen, D. Arnold, and K. Wendel-Mitoraj, "Local indicators of spatial autocorrelation (lisa): Application to blind noise-based perceptual quality metric index for magnetic resonance images." *Journal of imaging*, vol. 5, no. 1, pp. 1–23, 2019. DOI:10.3390/jimaging5010020

[24] M. A. Oliver, "The variogram and kriging," Springer, Berlin, Heidelberg, 2010, pp. 319–352. ISBN 978-3-642-03646-0. DOI:10.1007/978-3-642-03647-7_17

[25] C. V. Deutsch, "Geostatistics," Academic Press, 2003, pp. 697–707. ISBN 978-0-12-227410-7. DOI:10.1016/B0-12-227410-5/00869-3

[26] P. Singh and P. Verma, "A comparative study of spatial interpolation technique (idw and kriging) for determining groundwater quality," Elsevier, 2019, pp. 43–56. ISBN 978-0-12-815413-7. DOI:10.1016/B978-0-12-815413-7.00005-5

[27] A. Soltani and S. Askari, "Exploring spatial autocorrelation of traffic crashes based on severity," *Injury*, vol. 48, no. 3, pp. 637–647, 2017. DOI:10.1016/j.injury.2017.01.032

[28] A. Getis, "Reflections on spatial autocorrelation," *Regional Science and Urban Economics*, vol. 37, no. 4, pp. 491–496, 2007. DOI:10.1016/j.regsciurbeco.2007.04.005

[29] N. M. Huda, N. Imro'ah, and R. Mailanda, "Spatial autocorrelation using moran's index to map the confirmed positive of covid-19 cases in java," *AIP Conf. Proc.*, vol. 2588, no. 1, p. 050006, 2023. DOI:10.1063/5.0112014

[30] X. Zhou and H. Lin, "Geary's c," Springer, 2008, pp. 329–330. ISBN 978-0-387-30858-6. DOI:10.1007/978-0-387-35973-1_446

[31] F. Rossi and G. Becker, "Creating forest management units with hot spot analysis (getis-ord gi*) over a forest affected by mixed-severity fires," *Australian Forestry*, vol. 82, no. 4, pp. 166–175, 2019. DOI:10.1080/00049158.2019.1678714

[32] D. R. S. Saputro, Y. Widyaningsih, P. Widyaningsih, Sutanto, and Widiastuti, "Spatio-temporal patterns of dengue hemorrhagic fever (dhf) cases with local indicator of spatial association (lisa) and cluster map at areas risk in java-bali indonesia," *AIP Conf. Proc.*, vol. 2326, no. 1, p. 020027, 2021. DOI:10.1063/5.0040334

[33] N. M. Huda, U. Mukhaiyar, and U. S. Pasaribu, "Forecasting dengue fever cases using autoregressive distributed lag model with outlier factor," *AIP Conf. Proc.*, vol. 2268, no. 1, p. 020005, 2020. DOI:10.1063/5.0018450

[34] A. James and V. Tripathi, "Time series data analysis and arima modeling to forecast the short-term trajectory of the acceleration of fatalities in brazil caused by the corona virus (covid-19)," *PeerJ*, vol. 9, p. e11748, 2021. DOI:10.7717/peerj.11748

[35] N. M. Huda and N. Imro'ah, "Determination of the best weight matrix for the generalized space time autoregressive (gstar) model in the covid-19 case on java island, indonesia," *Spatial Statistics*, vol. 54, p. 100734, 2023. DOI:10.1016/j.spasta.2023.100734

[36] O. J. Watson, G. Barnsley, J. Toor, A. B. Hogan, P. Winskill, and A. C. Ghani, "Global impact of the first year of covid-19 vaccination: a mathematical modelling study," *The Lancet Infectious Diseases*, vol. 22, no 9, pp. 1293–1302, 2022. DOI:10.1016/S1473-3099(22)00320-6

[37] M. Manaqib, M. Mahmudi, and G. Prayoga, "Mathematical Model and Simulation of the Spread of COVID-19 with Vaccination, Implementation of Health Protocols, and Treatment," *Jambura Journal of Biomathematics (JJBM)*, vol. 4, no. 1, pp. 69–79, 2023. DOI:10.34312/jjbm.v4i1.19162

[38] F. Firmansyah and Y. M. Rangkuti, "Sensitivity Analysis and Optimal Control of Covid 19 Model," *Jambura Journal of Biomathematics (JJBM)*, vol. 4, no. 1, pp. 95–102, 2023. DOI:10.34312/jjbm.v4i1.19025

[39] S. O. S. P. Ahaya, E. Rahmi, and N. Nurwan, "Analisis dinamik model SVEIR pada penyebaran penyakit campak," *Jambura Journal of Biomathematics (JJBM)*, vol. 1, no. 2, pp. 57–64, 2020. DOI:10.34312/jjbm.v1i2.8482

[40] S. M. Moghadas, T. N. Vilches, K. Zhang, C. R. Wells, A. Shoukat, B. H. Singer, L. A. Meyers, K. M. Neuzil, J. M. Langley, M. C. Fitzpatrick, and A. P. Galvani, "The impact of vaccination on covid-19 outbreaks in the united states." *Clinical Infectious Diseases*, vol. 73, no. 12, pp. 2257–2264, 2021. DOI:10.1093/cid/ciab079

[41] G. E. P. Box, G. M. Jenkins, G. C. Reinsel, and G. M. Ljung, "Time Series Analysis: Forecasting and Control, 5th Edition," Wiley, 2015, p. 712. ISBN 978-1-118-67491-8